Near-Field Scattering by Physical Theory of Diffraction and Shooting and Bouncing Rays

Shyh-Kang Jeng, *Member, IEEE*

***Abstract*— This paper will propose a method to compute the near-field RCS and Doppler spectrum of a target when the distances to antennas are comparable to the target size. By dealing with a small piece of the target surface at a time, the transmitting antenna, and the receiving antenna are in the far-field zone of the small piece of the induced currents. And the electromagnetic field produced by this small piece of induced currents can be written as a spherical wave. Sum up all spherical waves produced by every small piece of induced currents and we can obtain the total scattered field at the receiving antenna. The physical theory of diffraction (PTD) and the method of shooting and bouncing rays (SBR) are modified to evaluate the received signals. Numerical results based on these techniques are obtained and discussed. The formulation in this paper applies the simple concepts of "equivalent" image and vector effective height, which are believed to be novel.**

***Index Terms*— Electromagnetic scattering, geometrical theory of diffraction, physical theory of diffraction.**

I. Introduction

THE problem of electromagnetic wave scattering is very important in defense applications. The research on this topic was mostly centered on far-field analysis: assume an incident plane wave, compute its scattered field due to the scatterer, and evaluate the radar cross section (RCS) of the scatterer. When the transmitting and receiving antennas are far from the scatterer, the incident wave can be approximated by a plane wave and the scattered far field can be regarded as the radiation far field due to the induced currents on the scatterer, the far-field analysis thus applies. However, in practical applications, there are many situations that the distance between the transmitting antenna and the scatterer is not large enough to treat the field arriving the scatterer as a plane wave and the relative motion between the antennas and scatterer will produce Doppler frequency shift. In these conditions the far-field analysis is not valid and a near-field analysis is necessary.

Most RCS papers on academic journals are related to the far-field analysis. I believe that much research on near-field analysis must have been done, but is difficult to find in academic journals because of its military value. The few near-field studies that the author knows are the NcPTD code [1] and the Cpatch code [10] developed in DEMACO. The basic idea for NcPTD is given as the following: for the near-field scattering problems to be considered, the transmitting antenna is close to the scatterer, but the distance is still much larger than the wavelength and the antenna size so that the field incident to the scatterer is still in the far-field zone of the transmitting antenna. This assumption enables us to approximate the incident field as a spherical wave, not a plane wave. This incident wave induces electric and magnetic currents on the scatterer and the induced currents generate the scattered field. Assume that the receiving antenna is also close to the scatterer such that the receiving antenna falls in the near field of the whole induced currents on the scatterer. This makes the analysis difficult. But if each time we deal with only a small piece of induced currents, the receiving antenna is in the far-field zone of the small piece of induced currents. Thus, the electromagnetic field produced by this small piece of induced currents can be written as a spherical wave. Sum up all spherical waves produced by the small pieces of induced currents and obtain the scattered electromagnetic field at the receiving antenna. During this process notice that the distance from each small piece of induced currents to the receiving antenna is finite and different. This is much different from the far-field analysis in which the distance from the scatterer to the receiving antenna is assumed infinity. However, in [1] only the physical theory of diffraction (PTD) is modified to deal with near-field scattering of convex scatterers. The method of shooting and bouncing rays (SBR), which is useful in evaluating the far-field RCS of concave targets, was not included. In the Cpatch code, however, both PTD and SBR are applied to compute the antenna coupling in complex environments. Nonetheless, the formulae in [1] are not explicit. Also, the equations and results of Cpatch cannot be found in academic journals.

This paper will apply a unified point of view to express explicit PTD and SBR formulas for near-field RCS problems. Some numerical results and discussions will be given. This formulation using the simple concepts of equivalent "image" and vector effective height, which will be introduced in later sections should be novel, although they must be equivalent to those utilized in developing NcPTD and Cpatch.

II. Statement of Problem

Assume that a missile carrying a lossless transmitting antenna and a lossless receiving antenna approaches a perfect-electric-conductor target in free-space (Fig. 1). For simplicity, assume that the target is composed of triangular facets. This assumption is rather general, because the surface of a scatterer

Manuscript received January 30, 1997; revised July 10, 1997. This work was supported by the National Science Council, Taiwan, R.O.C., under Contract CS85-0210-D002-012.

The author is with the Department of Electrical Engineering, National Taiwan University, Taipei, Taiwan, R.O.C.

Publisher Item Identifier S 0018-926X(98)02683-0.

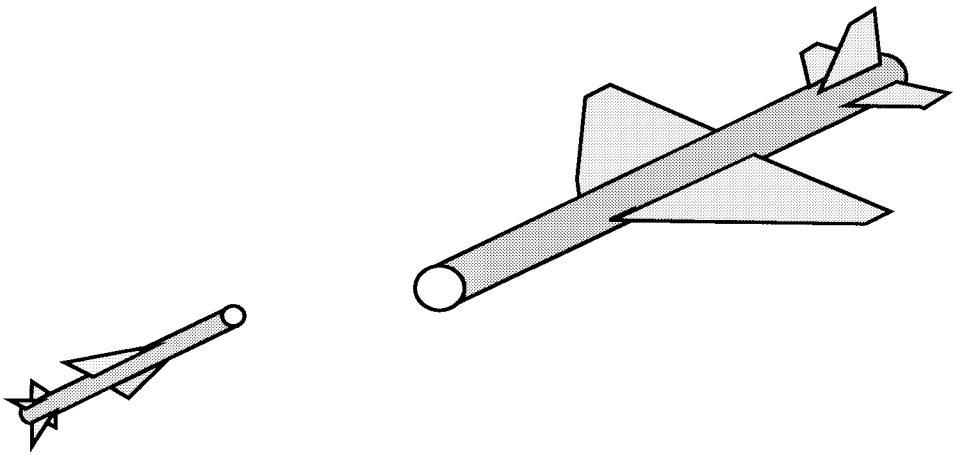

Fig. 1. Near-field scattering scenario.

can always be approximated by a set of triangular facets. Furthermore, provided that both of the missile and the scatterer are rigid bodies, and their motions in free-space can be decomposed into a translation and some rotations about three orthogonal axes.

Since the propagation speed of the electromagnetic wave is much larger than the speeds of the target and the missile, at any given instant we can determine the positions and orientations of the missile, target, and antennas. This scenario thus is "frozen" to let the electromagnetic wave be radiated from the transmitting antenna, scattered by the scatterer and received by the receiving antenna. The received signal is expressed by the received complex amplitude b_4 [3], [4]. Because the "frozen" scenario varies with time, the received b_4 is a function of time. By taking the Fourier transform of b_4 we can obtain the Doppler spectrum of the received signal. Besides, we can also find the near-field RCS of the first and the second kind [1], [4] at any moment. From [1], we know that the near-field RCS of the second kind approaches the far-zone RCS when the distance is large. And when isotropic antenna is used, the near-field RCS of the first kind can also be close to the far-field RCS in far zone. Finally, in the following analysis, the time-harmonic dependence $\exp(j\omega t)$ is assumed throughout.

III. Near-Field Physical Theory of Diffraction

A transmitting antenna Tx with input current I_T and vector effective antenna height (VEH) [2], [4] $\overline{h}_T$ is located at $\overline{r}_T$. Meanwhile, a receiving antenna Rx with vector effective antenna height $\overline{h}_R$ is located at $\overline{r}_R$. In addition to these two antennas, there is a scatterer composed of facets in free space. Let each facet be subdivided into small cells such that both distances from the target to Tx and to Rx are in the far-field zone of the induced currents on each cell. In other words, both $|\overline{r}-\overline{r}_T| \gg 2D^2/\lambda$ and $|\overline{r}-\overline{r}_R| \gg 2D^2/\lambda$ hold for any point $\overline{r}$ on a cell of size D. Under this condition, the incident electric field at $\overline{r}$ can be written as a spherical wave.

Select a point on a cell (say, the center of that cell) and denote this point as $\overline{r}_C$. Then, apply the far-field approximation $|\overline{r}-\overline{r}_T| \approx |\overline{r}_C-\overline{r}_T| = R_{CT}$ for magnitude and $|\overline{r}-\overline{r}_T| \approx R_{CT} - \hat{\zeta}_C \cdot \overline{R}_C$ for phase, where $\hat{\zeta}_C = (\overline{r}_T-\overline{r}_C)/|\overline{r}_T-\overline{r}_C|$ is a unit vector pointing from $\overline{r}_C$ to $\overline{r}_T$ and $\overline{R}_C = \overline{r}-\overline{r}_C$. This, plus the assumption that the corresponding pattern of Tx does not change much for points on a cell, enables us to approximate the incident field as a local plane wave

$$\overline{E}^{\,i}(\overline{r}) = \overline{E}^{\,i}_C\, e^{jk\hat{\zeta}_C\cdot\overline{R}_C} \tag{1a}$$

with

$$\overline{E}^{\,i}_C = -jk\eta\,\frac{e^{-jk|\overline{r}_C-\overline{r}_T|}}{4\pi\,|\overline{r}_C-\overline{r}_T|}\,I_T\overline{h}_{TC}. \tag{1b}$$

Here, k is the wave number and η is the intrinsic impedance of the free-space and the notation $\overline{h}_{TC}$ represents the VEH of Tx in the direction from Tx to $\overline{r}_C$. The related incident magnetic field is

$$\overline{H}^{\,i}(r) = -\frac{1}{\eta}\,\hat{\zeta}_C \times \overline{E}^{\,i}(\overline{r}). \tag{2}$$

Now approximate the induced electric current on the surface of the target by physical optics (PO) current

$$\begin{array}{ll} \overline{J}(\overline{r}) \approx 2\hat{n}\times\overline{H}^{\,i}(r) & \text{if } \overline{r} \text{ is illuminated} \\ \overline{J}(\overline{r}) \approx 0 & \text{if } \overline{r} \text{ is shadowed.} \end{array} \tag{3}$$

The unit vector $\hat{n}$ is the outward normal of the surface. The received field at $\overline{r}_R$ according to the PO current (3) on a cell with a center $\overline{r}_C$ then can be regarded as originating from an "image" electric current element $I_T\overline{h}^{PO}_C$ (Fig. 2). The corresponding equivalent VEH can be derived as

$$\overline{h}^{PO}_C = -\frac{jk}{2\pi}\left(\frac{R_{CR}+R_{CT}}{R_{CR}R_{CT}}\right)\hat{R}_{CR}\times\{\hat{R}_{CR} \times[\hat{n}\times(\hat{\zeta}_C\times\hat{h}_{TC})]\}\int_{\text{cell}} e^{jk(\hat{\zeta}_C+\hat{R}_{CR})\cdot\overline{R}'_c}\,ds'. \tag{4}$$

In (4), the integral over the cell in general can be integrated out if the cell is a polygon [5]. Notation R_{CR} represents the distance from $\overline{r}_C$ to Rx, and the unit vector $\hat{R}_{CR}$ is the direction from $\overline{r}_C$ to $\overline{r}_R$. Note that in (4) the equivalent VEH looks like a function of R_{CR} and R_{CT}, while in the original definition of VEH [2] it is independent of the distance. This difference is due to the following two reasons: First, the induced PO current on the cell is proportional to the incident field which is a spherical wave and has a factor of $1/R_{CT}$,

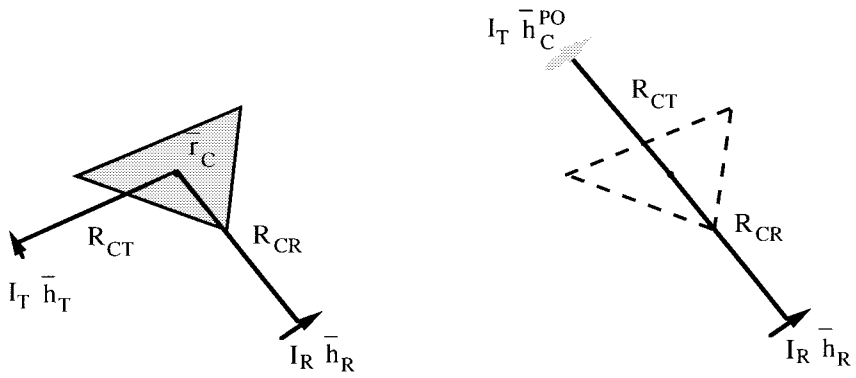

Fig. 2. Equivalence of PO current on a cell to an "image" electric current element.

while the antenna current in [2] is independent of the distances. Second, the ratio $R_{CR}/(R_{CR}+R_{CT})$ in (4) is used to ensure that the result can be imagined as an equivalent "image" $R_{CR}+R_{CT}$ away to calculate the corresponding b_4. It can approach a constant one when the distance R_{CR} is much larger than R_{CT}, which is the condition that [2] defines the vector effective height.

The received complex amplitude at Rx due to (4) can be easily given as [4]

$$b_4 = \frac{k^2}{16\pi^2}\left(\frac{\eta}{\sqrt{R_R R_T}}\right) \cdot \frac{e^{-jk(R_{CR}+R_{CT})}}{R_{CR}R_{CT}} \int_{\text{cell}} e^{jk(\hat{\zeta}_C+\hat{R}_{CR})\cdot\overline{R}'_C}\, ds' \cdot [-(\hat{n}\cdot\overline{h}_{TC})\,(\hat{\zeta}_C\cdot\overline{h}_{RC}) + (\hat{n}\cdot\hat{\zeta}_C)\,(\overline{h}_{TC}\cdot\overline{h}_{RC})]. \quad (5)$$

Here, R_R and R_T are antenna resistances of Tx and Rx, respectively. For monostatic case, $\hat{R}_{CR}=\hat{\zeta}_C$ and $\overline{h}_{TC}=\overline{h}_{RC}=\overline{h}_C$, (5) is simplified to

$$b_4 = \frac{k^2}{16\pi^2}\left(\frac{\eta}{R_T}\right)\frac{e^{-2jkR_{CR}}}{R_{CR}^2}\left[\int_{\text{cell}} e^{2jk\hat{\zeta}_C\cdot\overline{R}'_C}\, ds'\right] \cdot (\hat{n}\cdot\hat{\zeta}_C)(\overline{h}_C\cdot\overline{h}_C). \quad (6)$$

For PEC targets the diffraction is also important. The diffraction theory associated with the PO is the physical theory of diffraction (PTD). By PTD a set of equivalent electric and magnetic line currents is attached on the edge of the PEC wedge. Assume that each edge can be decomposed or approximated by many linear segment. The PTD edge currents on each segment are

$$\overline{J} = \frac{-1}{j\omega\mu_0} D_s(\overline{E}^{\,i}\cdot\hat{t})\,\hat{t}$$
$$\overline{M} = \frac{1}{j\omega\varepsilon_0} D_h(\overline{H}^{\,i}\cdot\hat{t})\hat{t}. \quad (7)$$

In (7) $\hat{t}$ is a unit vector along the edge segment, $\overline{E}^{\,i}$ and $\overline{H}^{\,i}$ are incident electric and magnetic fields, respectively, D_s and D_h are the Ufimtsev–Keller PTD diffraction coefficients [6].

The received field at $\overline{r}_R$ according to the PTD edge currents on an illuminated linear segment with a center $\overline{r}_C$ can also be treated as originating from an "image" electric current element $\overline{h}_T^{PTD}$ (Fig. 3), where

$$\overline{h}_C^{PTD} = \frac{1}{4\pi}\left(\frac{R_{CR}+R_{CT}}{R_{CR}R_{CT}}\right) d\,\text{sinc}\left[\frac{kd}{2}(\hat{\zeta}_C+\hat{R}_{CR})\cdot\hat{t}\right] \cdot [-\hat{R}_{CR}\times(\hat{R}_{CR}\times\hat{t})D_s(\overline{h}_{TC}\cdot\hat{t}) + (\hat{R}_{CR}\times\hat{t})D_h(\hat{\zeta}_C\times\overline{h}_{TC})\cdot\hat{t}]. \quad (8)$$

Here $R_{CT}=|\overline{r}_C-\overline{r}_T|$, $R_{CR}=|\overline{r}_C-\overline{r}_R|$, $\hat{\zeta}_C=(\overline{r}_T-\overline{r}_C)/R_{CT}$, and $\hat{R}_{CR}=(\overline{r}_R-\overline{r}_C)/R_{CR}$. We have also assumed that the length of the edge segment is d. The received complex amplitude due to (8) is [4]

$$b_4 = \frac{jk}{32\pi^2}\left(\frac{\eta}{\sqrt{R_R R_T}}\right) \cdot \frac{e^{-jk(R_{CR}+R_{CT})}}{R_{CR}R_{CT}}\, d\,\text{sinc}\left[\frac{kd}{2}(\hat{\zeta}_C+\hat{R}_{CR})\cdot\hat{t}\right] \cdot [-D_s(\overline{h}_{TC}\cdot\hat{t})(\hat{R}_{CR}\times\hat{t}) + D_h(\hat{\zeta}_C\times\overline{h}_{TC})\cdot\hat{t}\hat{t}] \cdot (\overline{h}_{RC}\times\hat{R}_{CR}). \quad (9)$$

For monostatic case, $\hat{R}_{CR}=\hat{\zeta}_C$ and $\overline{h}_{TC}=\overline{h}_{RC}=\overline{h}_C$ and (9) is simplified to

$$b_4 = \frac{jk}{32\pi^2}\left(\frac{\eta}{R_T}\right)\frac{e^{-2jkR_{CR}}}{R_{CR}^2}\, d\,\text{sinc}(kd\hat{\zeta}_C\cdot\hat{t}) \cdot \{D_s(\overline{h}_C\cdot\hat{t})^2 - D_h[(\hat{t}\times\hat{\zeta}_C)\cdot\overline{h}_C]^2\}. \quad (10)$$

IV. Near-Field Shooting and Bouncing Rays

The PTD introduced in last section is applicable for single reflection/diffraction. If multiple reflections become significant, we have to use the SBR technique. The original SBR technique deals with only far-field scattering problem [7], thus, we have to modify it to handle near-field scattering problems.

First of all, the surface of the target is divided into many small cells. By connecting the transmitting antenna Tx and every small cells, we check if each connected line is blocked. If a connected line is not blocked, we can obtain a corresponding ray tube of triangular cross section. These ray tubes will reflect over the scatterer surface. The propagation of the ray tubes can be determined by tracing the center rays.

A ray tube launched from $\overline{r}_T$ will experience many reflections. Let $\overline{r}_q$ denote the qth reflection point of the center ray, and $\overline{r}_0=\overline{r}_T$. Besides, symbol l_q represents the ray path length from $\overline{r}_T$ to $\overline{r}_q$. For the qth bounce of a ray tube, the effect

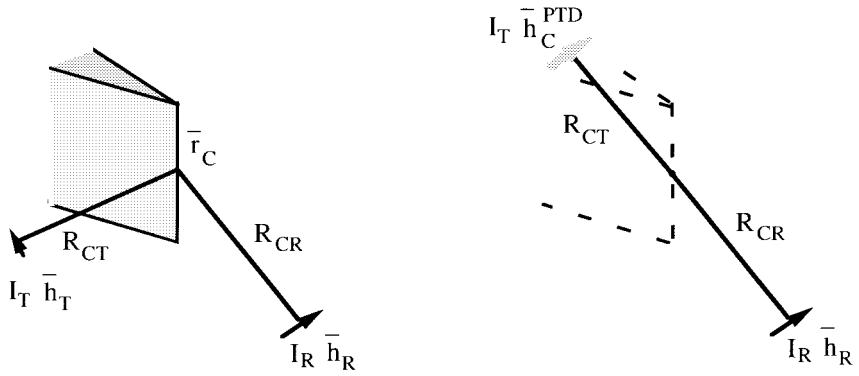

Fig. 3. Equivalence of PTD edge currents on an edge segment to an "image" electric current element.

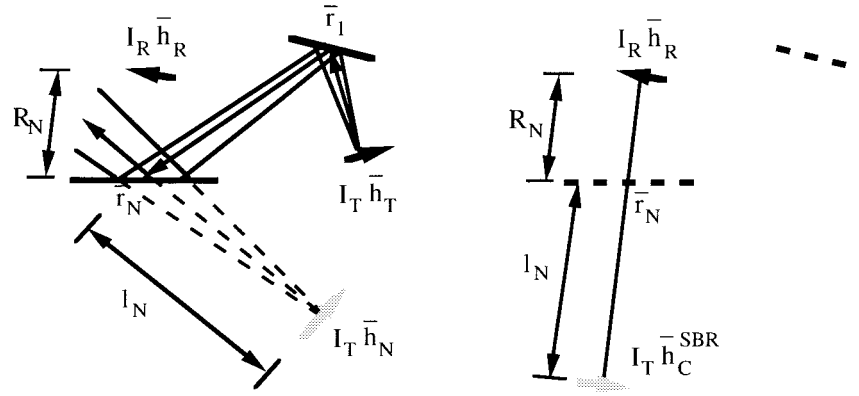

Fig. 4. Equivalence of surface currents due to the last bounce to an "image" electric current element.

of reflection can be substituted by an image antenna of vector effective antenna height $\overline{h}_q$. The recursive relationship between $\overline{h}_q$ and $\overline{h}_{q-1}$ can be derived as

$$\overline{h}_q = -\overline{h}_{q-1} + 2(\hat{n}_q \cdot \overline{h}_{q-1})\hat{n}_q \tag{11}$$

where $\hat{n}_q$ is the unit normal vector of the target at $\overline{r}_q$.

Repeat tracing the center ray until no more reflection occurs. Let there be N reflections, the VEH of the last image is $\overline{h}_N$, and the intersection area of the ray tube and the target around the last reflection point $\overline{r}_N$ is S_N. From the idea of image the position of $\overline{h}_N$ can be determined as

$$\overline{r}'_N = \overline{r}_N - \ell_N \hat{\zeta}_N \tag{12}$$

and the equivalent surface currents due to reflected fields on S_N are

$$\begin{aligned} \overline{J} &= \hat{n}_N \times \overline{H}_N \\ \overline{M} &= \overline{E}_N \times \hat{n}_N \end{aligned} \tag{13}$$

where $\hat{n}_N$ is the outward normal vector on S_N, $\overline{E}_N$, and $\overline{H}_N$ are the field generated by $\overline{h}_N$. The field received at $\overline{r}_R$ due to (13) then can be regarded as produced by an "image" electric current element $\overline{h}_C^{\mathrm{SBR}}$ (Fig. 4), where

$$\begin{aligned} \overline{h}_C^{\mathrm{SBR}} = \frac{jk}{4\pi}\left(\frac{R_N + \ell_N}{R_N \ell_N}\right) \int_{S_N} e^{jk(\hat{R}_N - \hat{\zeta}_N)\cdot \overline{R}'_N}\, ds' \\ \cdot (\hat{R}_N \times \{\hat{R}_N \times [\hat{n}_N \times (\hat{\zeta}_N \times \overline{h}_N)]\} \\ + \hat{R}_N \times (\hat{h}_N \times \hat{n}_N)). \end{aligned} \tag{14}$$

Note that in (14) $R_N = |\overline{r}_R - \overline{r}_N|$, $\hat{R}_N = (\overline{r}_R - \overline{r}_N)/|\overline{r}_R - \overline{r}_N|$. The received complex amplitude due to a ray tube is [4]

$$\begin{aligned} b_4 = -\frac{k^2}{32\pi^2}\left(\frac{\eta}{\sqrt{R_R R_T}}\right)\frac{e^{-jk(R_N+\ell_N)}}{R_N \ell_N} \\ \cdot \int_{S_N} e^{jk(\hat{R}_N - \hat{\zeta}_N)\cdot \overline{R}'_N}\, ds' [(\overline{h}_R \times \hat{R}_N) \cdot (\overline{h}_N \times \hat{n}_N) \\ + (\hat{n}_N \times \overline{h}_R) \cdot (\hat{\zeta}_N \times \overline{h}_N)]. \end{aligned} \tag{15}$$

Note that if only single bounce occurs, (15) can be reduced to the PO result (5).

The total received complex amplitude b_4 due to the scatterer then is the superposition of the contributions from all PO cells, PTD edge segments, and SBR ray tubes. Note, however, remember to exclude the single-bounce contribution in the SBR computation, when PO contribution has been included. Note that the divergence factor for each bounce is not included, because the target has been assumed to be composed of facets. Suppose that the scatterer were composed of curved surface patches, the divergence factor should be multiplied in the expressions (11) and (14). Since the divergence factor makes the program complicated (i.e., the treatment of the curvatures and the problem of caustics), it is not dealt with in this work. The code Cpatch, however, can handle the divergence factor for curved surfaces [10].

V. Numerical Results and Discussions

Based on the theoretical analysis methods proposed in former chapters, we have developed a FORTRAN program

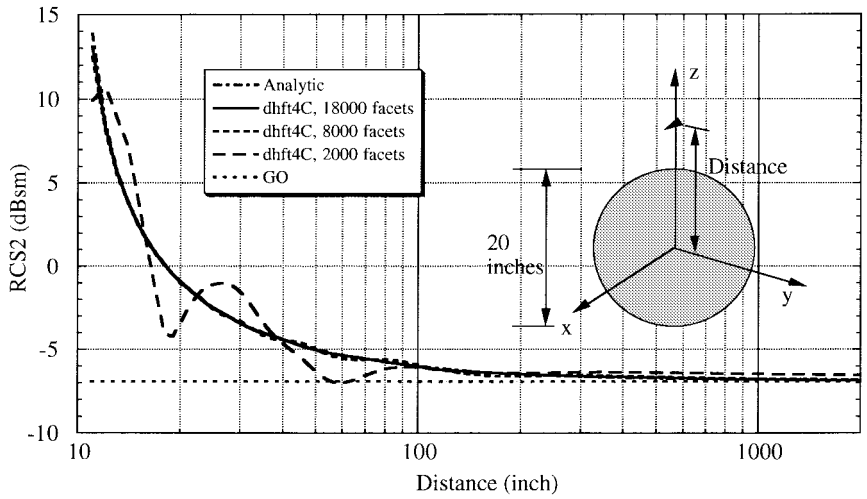

Fig. 5. Near-field RCS σ_2 of a PEC sphere of 10 in radius at different distance d.

dhft4C (the acronym dhft stands for **d**iscrete **h**igh **f**requency **t**echnique) to compute the received complex amplitude b_4 and the near-field radar cross sections of the first kind σ_1 and the second kind σ_2 [1], [4]. The computed b_4 as a function of time may be processed to produce Doppler spectrum through discrete Fourier transform. For brevity, all numerical examples given here are simply monostatic. In computing σ_1 and σ_2, respectively, the origin of the coordinate system is placed in the scatterer, and is used to calculate the distance and to determine the antenna gain.

To verify dhft4C, we first deal with the scattering problem of a PEC sphere of radius 10 in at 10 GHz. In this problem, the distance between an x-directed electric current element (i.e., a Hertzian dipole) located on the z axis and the center of the sphere (as the origin of the coordinate system) is denoted as r_0. The analytic solution of this problem can be found in [8]. On the other hand, this problem is also solved by dhft4C, where the sphere is approximated by 2000, 8000, and 18 000 triangular facets using the algorithm presented in [9] to ensure that every facet is with almost the same size. The computed σ_2 in dBsm from both approaches are shown in Fig. 5. Also plotted in Fig. 5 is the far-field GO RCS πa^2, where a is the radius. From the curves exhibited in Fig. 5, we can find that both the analytic solution curve and the dhft4C result curves are almost overlapped when the facet size is small enough, which means that the error of our approach can be very small for the distance r_0 ranging from 11 in (very close to the sphere) to 2000 in (far away from the sphere). From the same figure we also discover that while both the analytic solution curve and the dhft4C result curves approach the GO limit as the distance r_0 increases, the near-field RCS can deviate much from the far-field GO RCS when the distance r_0 is not large enough, which shows that the near-field scattering behavior can be very different from the far-field one, if the far-field condition does not hold.

For edge diffraction and multiple reflections, the author has tested several common cases like a rectangle plate, a dihedral, and a trihedral. Since the near-field RCS's of these targets are not available to me, I can only check the convergence by

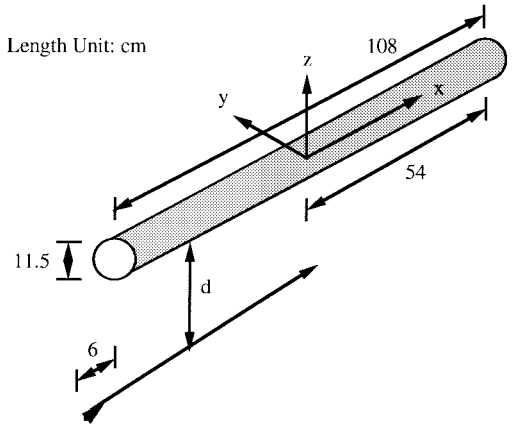

Fig. 6. Near-field scattering of a PEC cylinder. The antenna moves along the x direction in the speed of 1.0 cm/ms.

varying the size of the facets/edge segments and the number of ray tubes. The results are satisfactory. I have also found that when the distances increase such that the far-field criterion of the whole scatterer can be satisfied, the computed near-field RCS of the second kind coincide with the far-field RCS computed by a far-field RCS code. These support the validity of the code dhft4C.

Fig. 6 displays another case where a 10-GHz antenna moves at the speed of 1 cm/ms beneath a circular cylinder of radius 5.75 cm and length 108 cm. Assume that the direction of the antenna motion is parallel to the axis of the cylinder (the x axis), the distance between the trajectory of the antenna and the cylinder axis is d, and the initial x coordinate of the antenna is 6 cm from the x coordinate of the front end of the cylinder. First, let us consider an x-directed isotropic antenna. Then, in Fig. 7, we show the Doppler spectra under different d. In our computation, we sample the received b_4 every millisecond and, thus, we need consider only the Doppler spectra for Doppler frequency less than 0.5 KHz by Nyquest sampling theorem. On the other hand, the spectra are obtained by doing discrete Fourier transform to all 120 b_4 data in 120 ms. Since in the far zone the cylinder is like a point scatterer in the same z direction, if we can do the Fourier transform to the data from

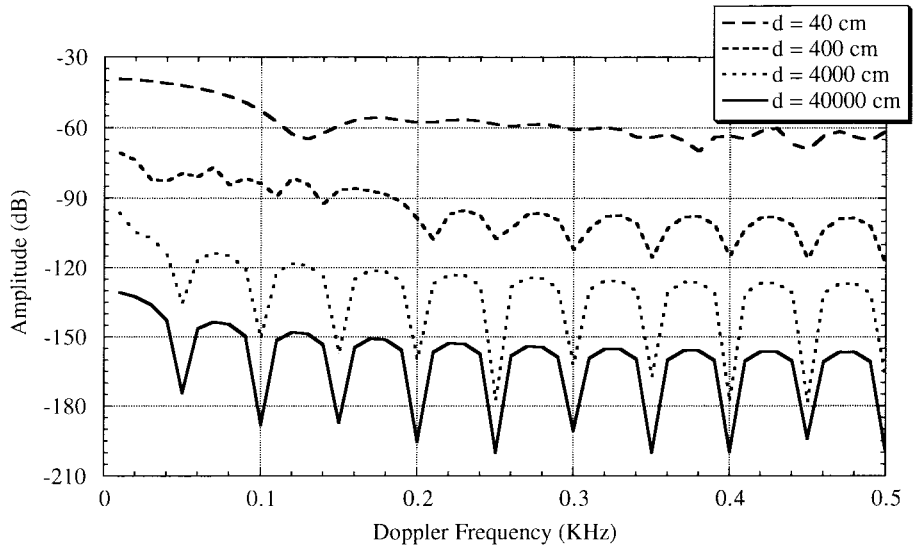

Fig. 7. Doppler spectrum of a PEC cylinder due to a moving isotropic antenna.

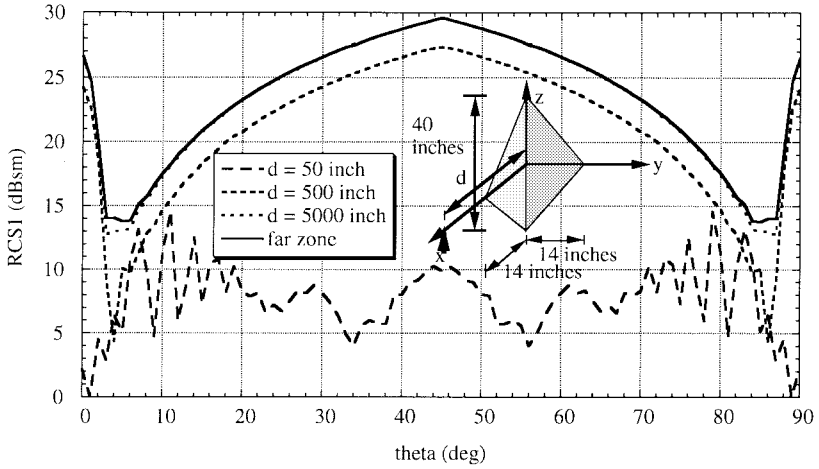

Fig. 8. Near-field RCS σ_1 of a dihedral made of two triangular PEC plates. The z-polarized isotropic antenna is on the x axis.

$t = -\infty$ to $t = \infty$, the received signal does not change with time and the spectrum for $d = 40\,000$ cm will very similar to a sharp spike at 0 Hz. However, in our evaluation, only the data within the 120 ms are used and, thus, we can find the famous sinc function pattern for the computed Doppler spectrum at $d = 40\,000$ cm. When d is smaller, the variation of the received signals become stronger with time and the obtained Doppler spectra thus are flatter. Especially, when $d = 40$ cm, the "bandwidth" of the Doppler spectrum expands to 0.12 KHz, which is almost three times of that of the Doppler spectrum when $d = 40\,000$ cm.

Another example is the scattering of a dihedral made of two orthogonal triangular PEC plates illuminated by an isotropic antenna located on the x axis. The four vertices of this dihedral are given as (0, 0, -20), (0, 0, 20), (14, 0, 0), and (0, 14, 0), where the coordinates are in inches. The dihedral rotates about the z axis and only the monostatic σ_1 in the range of $0° \leq \phi \leq 90°$ where the double reflection is dominant is shown in Fig. 8. The curves obtained for various distance d also reveal that when d is large the σ_1 is again reduced to the far-field RCS, which was calculated by a far-field RCS code. From these curves we also find that the monostatic σ_1 around $\phi = 45°$ is much smaller when d is not so large, because in the near-field zone most of the launched rays cannot return to the original directions, which results in a smaller monostatic σ_1. On the contrary, in the far-field zone all generated rays are parallel and will go back to the direction of incidence after two bounces, which produces a large monostatic RCS.

Finally, we consider a simplified aircraft model 108-cm long, shown in Fig. 9, and compute σ_1 for a y-polarized isotropic antenna located on the x axis and the target rotate on the x–y plane. In Fig. 10, the dashed line is for σ_1 of a far-field situation (distance to the target origin is 50 000 cm), and the solid line is for a near-field case (distance to the target origin is 500 cm). Note that there are an inlet in the head and an outlet in the tail of the model, hence, multiple reflection is significant for incident rays entering the inlet and the outlet. This can be observed for ϕ around 0 and 180°, for if the head and the tail were closed by circular plates, the RCS lobe will be very sharp in the head and the tail directions. Also, we can

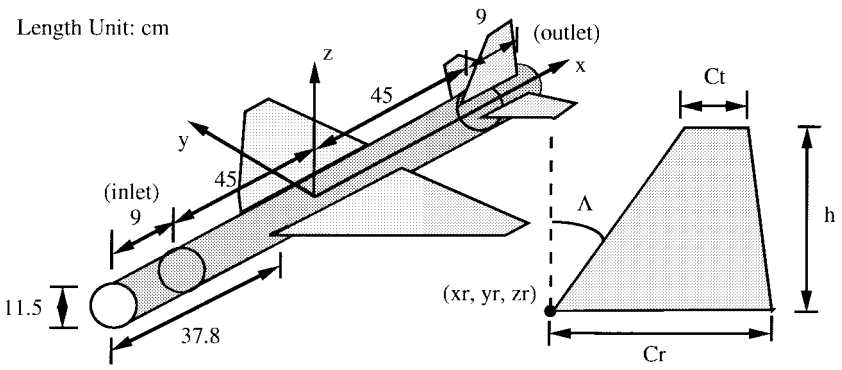

	xr	yr	zr	Cr	Ct	h	Λ
Right Wing	-16.2	5.75	0.0	43.7	2.7	27.0	56.6°
Right H-Tail	37.5	5.75	0.0	16.5	3.5	11.73	60.6°
V-Tail	37.5	0.0	5.75	16.5	3.5	11.73	60.6°

Fig. 9. A simplified aircraft model.

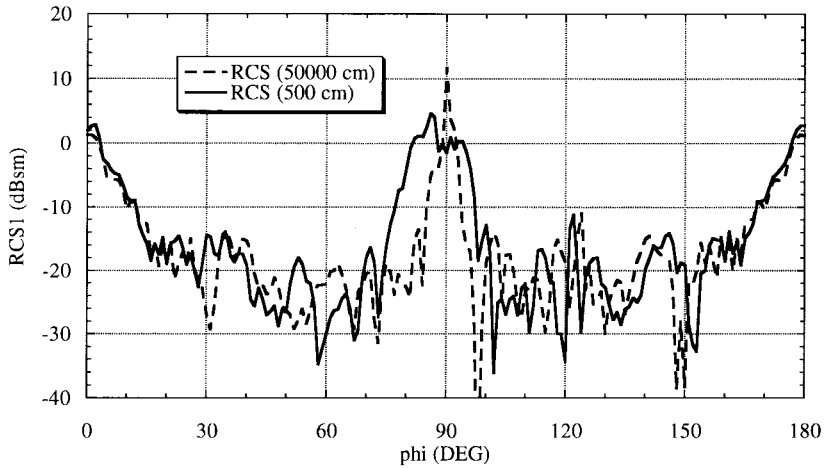

Fig. 10. Near-field RCS σ_1 of the simplified aircraft model at different distances.

find that the lobe around 90° becomes wider when the antenna is near the target. This is also comprehensible, since in the far-field case, all rays are almost parallel, and there is a strong and sharp return at $\phi = 90°$, while in the near-field case, the rays are no longer parallel and the sharp lobe is changed to a wider and lower lobe structure.

VI. Conclusions

We have successfully developed a near-field RCS analysis code to analyze the near-field scattering of a dynamic target. PTD and SBR have been used to calculate the received complex amplitude b_4. Both of the antenna and the target can move and rotate. From the computed received complex amplitude b_4, the near field RCS's of two kinds of definitions and the Doppler spectrum can be obtained. We have validated our theory first by comparing the near-field RCS of a PEC sphere with the analytical solution. We also have checked the numerical convergence and verified the behavior of the near-field RCS at far zone. In addition, we observed that the Doppler spectrum spreads out when the antenna is close to the target. This theory can be extended to handle targets with dielectric radomes or coated surfaces. For the target modeled by curved surfaces, more efforts are needed to derive PO formulas and include the effect of divergence factor in SBR.

Acknowledgment

The author would like to thank Prof. M. Ouhyoung, C. C. Chen, and J. R. Jeng of the Department of Computer Science and Information Engineering, National Taiwan University, for developing a wonderful Graphic User Interface for dhft4C, which is very useful in checking input data and visualizing the reflections of rays.

References

[1] S. W. Lee, H. T. G. Wang, and G. Labarre, "Near-field RCS computation," *Appendix in the Manual for NcPTD-1.2*, S. W. Lee, writer. Champaign, IL: DEMACO, 1991.

[2] P. K. Park and C. T. Tai, "Receiving antennas," in *Antenna Handbook*, Y. T. Lo and S. W. Lee, Eds. New York: Van Nostrand Reinhold, 1988, ch. 6.

[3] S. W. Lee, "Fundamentals," in *Antenna Handbook*, Y. T. Lo and S. W. Lee, Eds. New York: Van Nostrand Reinhold, 1988, ch. 2.
[4] M. Ouhyoung and S. K. Jeng, "Analysis and visualization of the near-field scattering spectrum of a dynamic target," Final Rep. for Nat. Sci. Council, Contract CS85-0210-D002-012, Nat. Taiwan Univ., Taipei, Taiwan, Sept. 1995.
[5] S. W. Lee and R. Mittra, "Fourier transform of a polygonal shape function and its applications in electromagnetics," *IEEE Trans. Antennas Propagat.*, vol. AP-31, pp. 99–103, Jan. 1983.
[6] P. H. Pathak, "Techniques for high-frequency problems," in *Antenna Handbook*, Y. T. Lo and S. W. Lee, Eds. New York: Van Nostrand Reinhold, 1988, pp. 4-102–4-115.
[7] H. Ling, R. C. Chou, and S. W. Lee, "Shooting and bouncing rays: Calculating the RCS of an arbitrarily shaped cavity," *IEEE Trans. Antennas Propagat.*, vol. 37, pp. 194–205, Feb. 1989.
[8] D. L. Sengupta, "The sphere," in *Electromagnetic and Acoustic Scattering by Simple Shapes*, J. J. Bowman, T. B. A. Senior, and P. L. E. Uslenghi, Eds. New York: Hemisphere, 1987, ch. 10.
[9] S. H. Chen and S. K. Jeng, "An SBR/image approach for indoor radio propagation in a corridor," *Trans. IEICE Electron.*, vol. E78-C, no. 8, pp. 1058–1062, Aug. 1995.
[10] S. W. Lee, J. E. Baldauf, and R. A. Kipp, "Cpatch overview," description of capability of code Cpatch developed by DEMACO, 1994.

Shyh-Kang Jeng (M'87) was born in I-Lan, Taiwan, R.O.C., on May 6, 1957. He received the B.S.E.E. and Ph.D. degrees from National Taiwan University, Taipei, Taiwan, R.O.C., in 1979 and 1983, respectively.

In 1981, he joined the faculty of the Department of Electrical Engineering, National Taiwan University, Taipei, where he is now a Professor. From 1984 to 1985 he was an Electronic Data Processing Officer and Instructor of information system analysis and design at National Defense Management College, Chung-Ho, Taiwan, R.O.C. From 1985 to 1993, he visited University of Illinois, Urbana-Champaign, as a Visiting Research Associate Professor and a Visiting Research Professor several times. His current research interest is in three-dimensional sound, music systems, indoor and outdoor channel modeling for wireless communications, and electromagnetic scattering analysis and visualization.